Cell Reports

The *Drosophila* Small Conductance Calcium-Activated Potassium Channel Negatively Regulates Nociception

Graphical Abstract

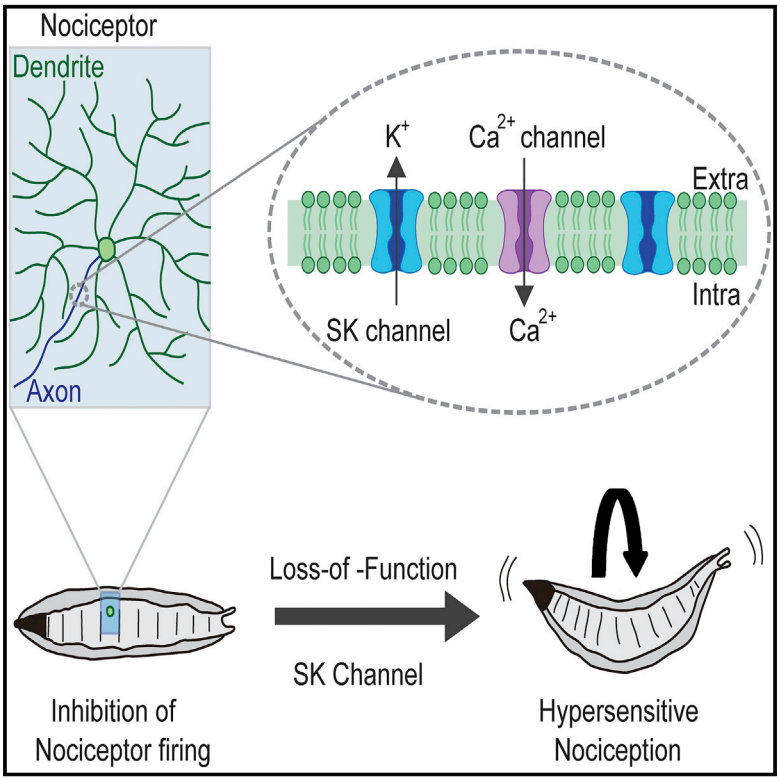

Highlights

- Specific potassium channels regulate nociceptor excitability
- SK channels have a critical function in nociception
- SK channels specifically localize to sensory axons
- SK channels are not detectable in sensory dendrites

Authors

Kia C.E. Walcott, Stephanie E. Mauthner, Asako Tsubouchi, Jessica Robertson, W. Daniel Tracey

Correspondence

dtracey@indiana.edu

In Brief

Walcott et al. performed a forward genetic screen and identify three potassium channel subunits that negatively regulate nociception in *Drosophila* larvae. In a more detailed investigation of the SK channel, null mutants, rescue experiments, optical recordings, and protein localization studies indicate a functional role for SK in nociceptor excitability.

Walcott et al., 2018, Cell Reports *24*, 3125–3132
September 18, 2018
https://doi.org/10.1016/j.celrep.2018.08.070

CellPress

Cell Reports
Report

The *Drosophila* Small Conductance Calcium-Activated Potassium Channel Negatively Regulates Nociception

Kia C.E. Walcott,[3,6] Stephanie E. Mauthner,[1,2,6] Asako Tsubouchi,[4,7] Jessica Robertson,[5] and W. Daniel Tracey,[1,2,4,5,8,*]
[1]Gill Center for Biomolecular Research, Indiana University, Bloomington, IN, USA
[2]Department of Biology, Indiana University, Bloomington, IN, USA
[3]Department of Pharmacology and Cancer Biology, Duke University Medical Center, Durham, NC, USA
[4]Department of Anesthesiology, Duke University Medical Center, Durham, NC, USA
[5]Department of Cell Biology, Duke University Medical Center, Durham, NC, USA
[6]These authors contributed equally
[7]Present address: Laboratory of Frontier Image Analysis, Graduate School of Arts and Sciences, The University of Tokyo, 3-8-1 Komaba, Meguro-ku, Tokyo 153-8902, Japan
[8]Lead Contact
*Correspondence: dtracey@indiana.edu
https://doi.org/10.1016/j.celrep.2018.08.070

SUMMARY

Inhibition of nociceptor activity is important for the prevention of spontaneous pain and hyperalgesia. To identify the critical K^+ channels that regulate nociceptor excitability, we performed a forward genetic screen using a *Drosophila* larval nociception paradigm. Knockdown of three K^+ channel loci, the *small conductance calcium-activated potassium channel* (*SK*), *seizure*, and *tiwaz*, causes marked hypersensitive nociception behaviors. In more detailed studies of *SK*, we found that hypersensitive phenotypes can be recapitulated with a genetically null allele. Optical recordings from nociceptive neurons showed a significant increase in mechanically activated Ca^{2+} signals in *SK* mutant nociceptors. SK is expressed in peripheral neurons, including nociceptive neurons. Interestingly, SK proteins localize to axons of these neurons but are not detected in dendrites. Our findings suggest a major role for SK channels in the regulation of nociceptor excitation and are inconsistent with the hypothesis that the important site of action is within dendrites.

INTRODUCTION

The sensation of pain is important for avoiding exposure to noxious environmental stimuli that have the potential to cause tissue damage. These stimuli are detected by nociceptors, which are the primary sensory neurons that detect noxious mechanical, noxious chemical, and/or noxious temperatures. Transduction of noxious thermal, mechanical, and chemical stimuli is initiated by sensory receptor ion channels, which depolarize the sensory neuron plasma membrane and trigger action potentials (Dubin and Patapoutian, 2010). In the absence of such stimuli, healthy nociceptors remain relatively silent, with little spontaneous activity (Ritter and Mendell, 1992; Xiang et al., 2010) due to the action of potassium (K^+) channels and chloride (Cl^-) channels, which oppose depolarizing sodium (Na^+) and calcium (Ca^{2+}) currents. Despite their importance in keeping nociceptive neurons silent, the identity of the K^+ channels that play the most critical roles in negatively regulating nociceptor excitability remains largely undetermined.

To identify these critical channels, we conducted a forward genetic screen using a modified *Drosophila* larval nociception paradigm that was optimized for detecting hypersensitive nociception phenotypes (Honjo et al., 2016).

RESULTS AND DISCUSSION

Tissue-Specific Knockdown of K^+ Channel Genes in *Drosophila* Uncovers Hypersensitive Thermal Nociception Phenotypes

A collection of transgenic RNAi strains from the Vienna *Drosophila* Resource Center (VDRC) and the Transgenic RNAi Project (TRiP) allow for *in vivo* tissue-specific gene silencing under control of the Gal4/UAS system (Dietzl et al., 2007; Brand and Perrimon, 1993; Ni et al., 2009). We identified 53 UAS-inverted repeat (UAS-IR) RNAi lines in these collections that targeted 34 K^+ channels with few predicted off-target effects (Table S1). All known *Drosophila* K^+ channels are represented in our assembled collection.

We first investigated the effects of knocking down the K^+ channels under control of the *GAL4109(2)80;UAS-Dicer2* (*md-Gal4*;*UAS-Dicer2*) driver strain. This strain drives UAS transgene expression in the class I, II, III, and IV md neurons (Gao et al., 1999). Evidence suggests that the major nociceptive function is mediated by the class IV md neurons, but class II and class III neurons are also involved (Hwang et al., 2007; Hu et al., 2017). The use of *UAS-Dicer2* in the driver strain results in more efficient gene silencing (Dietzl et al., 2007). To perform the screen, the *md-Gal4*;*UAS-Dicer2* driver strain was crossed to each of the 53 UAS-RNAi strains targeting the K^+ channels and the nocifensive escape locomotion (NEL) response latency

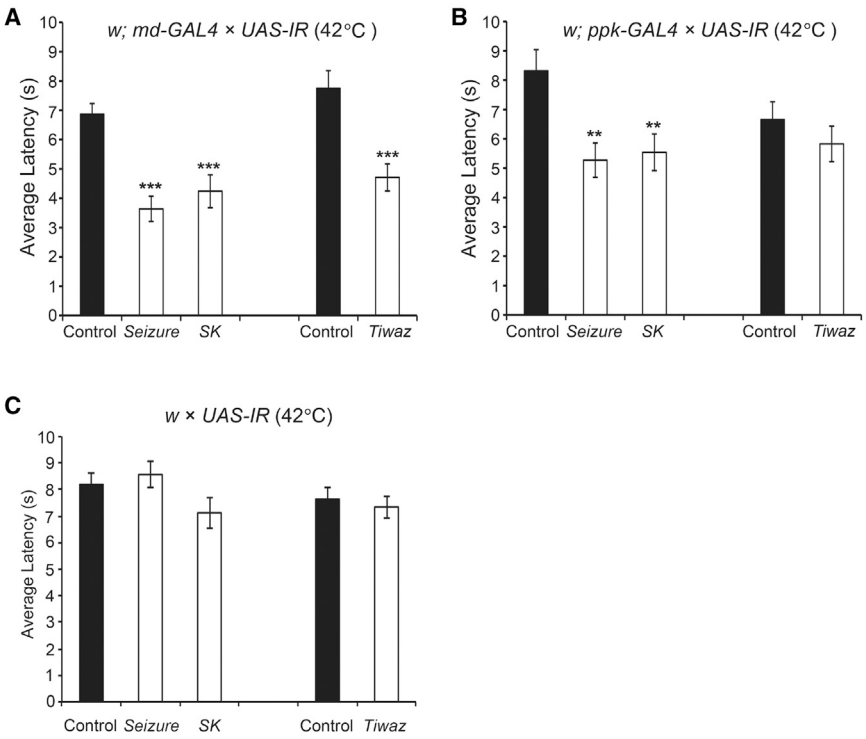

Figure 1. Thermal Nociception Responses of K^+ Channel Knockdown Larvae

(A) In response to a noxious temperature (42°C), larval crossed progeny from *w; md-Gal4; UAS-Dicer2* and *UAS-IR* lines targeting *seizure* (P{KK105733}v104698) or *SK* (P{KK107699}v103985) show reduced latency compared to control animals. One-way ANOVA with Dunnett's test, ***$p < 0.001$. Larval crossed progeny from *w; md-Gal4; UAS-Dicer2* and a *UAS-IR* line targeting *tiwaz* (P{TRiP.JF01867}) show hypersensitivity to 42°C noxious heat compared to control animals. Student's t test, ***$p < 0.001$.

(B) The average NEL latency of larval progeny from *w; ppk-Gal4; UAS-Dicer2* crossed to *UAS-IR* lines targeting *SK*, *seizure*, and *tiwaz* when stimulated with a 42°C probe. *SK-RNAi* and *seizure-RNAi* animals show reduced latency to perform nociception behaviors compared to control animals. One-way ANOVA with Dunnett's test, **$p < 0.01$. *tiwaz*-RNAi animals do not show significant hypersensitivity to noxious heat compared to control animals. Student's t test, $p = 0.29$. Data are presented as mean ± SEM.

(C) *UAS-IR* RNAi transgenes alone do not show thermal nociception defects. Control strains from the VDRC-KK and TRiP collections and RNAi transgenes targeting *SK*, *seizure*, and *tiwaz* were each crossed to the w^{1118} strain. No difference was detected relative to the control animals. One-way ANOVA with Dunnett's test. Similarly, animals carrying the *UAS-IR* transgene targeting *tiwaz* in the absence of the driver are not different from the control strain. Data are presented as mean ± SEM, see Table S2 for sample sizes.

of the larval progeny stimulated with a 42°C heat probe were measured. The crossed progeny from UAS-RNAi lines targeting three distinct K^+ channel subunits showed a significantly more rapid response relative to the genetic background control strain: the *small conductance calcium-activated potassium channel* (*SK*) (Abou Tayoun et al., 2011), the *seizure* channel (in the *ether-a-gogo* family) (Jackson et al., 1984), and the *tiwaz* gene (encodes a protein with homology to the potassium channel tetramerization domain) (Williams et al., 2014) (Figures 1A and 1C) (Table S2 reports all transgenic flies used in this study). Although phenotypes were not observed for other tested K^+ channels, this method for RNAi is prone to false negatives, so our screen cannot rule out potential involvement for other channels. To test whether the effects of the RNAi were specific to the nociceptive class IV sensory neurons, we next tested animals expressing UAS-RNAi targeting these three candidates under control of *ppk-Gal4*;*UAS-Dicer2* (Ainsley et al., 2003). The hypersensitive responses persisted in *SK*-RNAi and *seizure*-RNAi animals (Figures 1B and 1C).

SK Negatively Regulates Thermal Nociception Behavior

A prior pharmacological study on mammalian sensory neurons suggested an SK-mediated pathway for nociceptor excitability (Pagadala et al., 2013); however, the cellular role of this ion channel specifically in nociception remains largely unexplored and has not been verified with genetic mutants. The mammalian genome contains three genes that encode SK channel subunits (Köhler et al., 1996), while the *Drosophila* genome encodes only a single *SK* locus on the X chromosome (Abou Tayoun et al., 2011; Adelman et al., 2012; Köhler et al., 1996) that is 60 kb in length and is predicted to encode at least 14 distinct transcripts (Gramates et al., 2017) (Figure 2A [for simplicity, only two transcripts are shown]). The *Drosophila SK* locus has been found to mediate, a slow Ca^{2+}-activated K^+ current in photoreceptor neurons and muscle as well as playing a role in learning and memory (Abou Tayoun et al., 2011, 2012; Gertner et al., 2014). To further investigate the function of SK, we generated a DNA null mutant by deleting the gene with Flippase (FLP) and FLP recombination target (FRT)-containing transposons (Thibault et al., 2004; Parks et al., 2004) (Figures 2A, S1A, and S1B). Consistent with the hypothesis that SK is an important negative regulator of nociception, *SK* null mutants (*ΔSK*) showed a pronounced hypersensitive response at 42°C. These animals showed an average response latency to a 42°C stimulus of 3.2 s, which was significantly faster than the control background strain (Exelixis isogenic *white*) response of 6.2 s (Figure 2B).

To confirm that loss of SK was responsible for the nociception defect, we performed a genetic rescue experiment through transgenic insertion of an ~80-kb bacterial artificial chromosome (BAC) that covered the entire *SK* locus (Venken et al., 2006). The BAC transgenic flies were crossed into the *SK* genetic mutant background to create rescue animals containing either

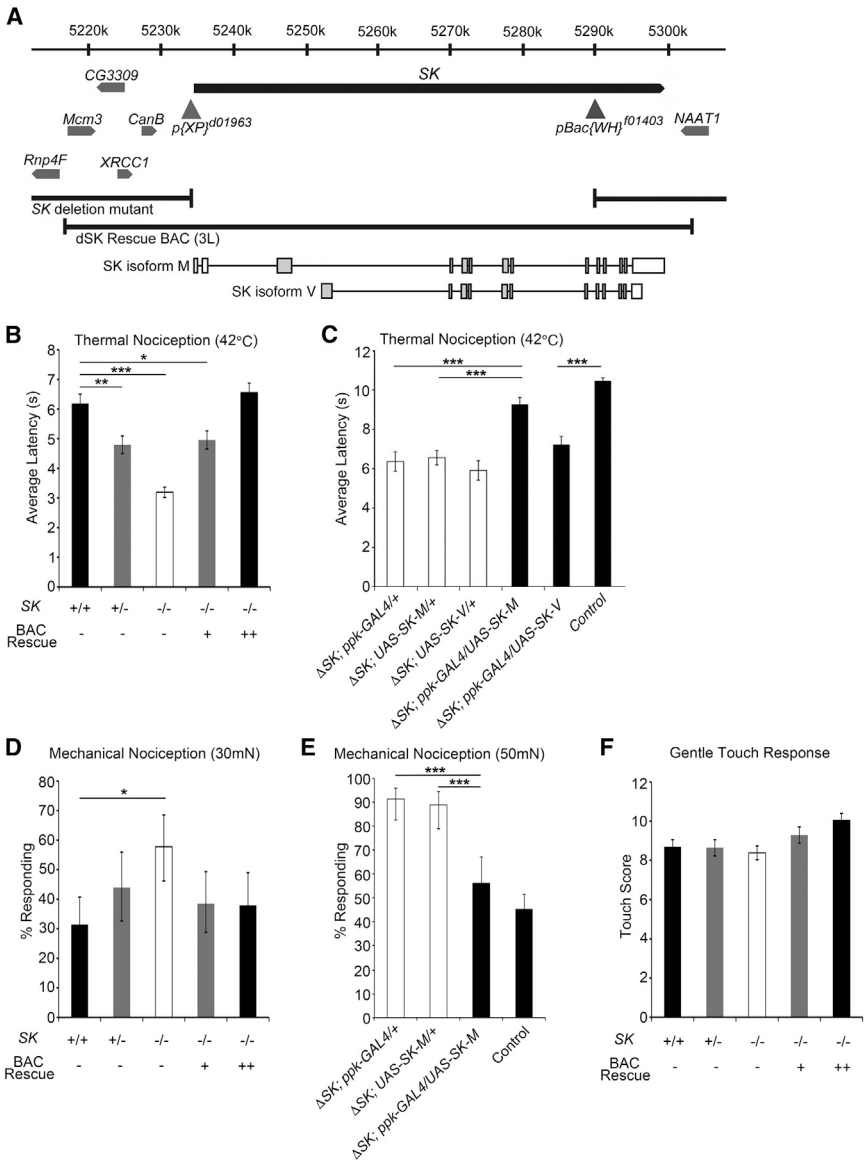

Figure 2. Expression of *SK* Rescues the Nociception Phenotypes

(A) Schematic representation of the genetic interval surrounding *SK* locus. The locations of *pBac* and P transposable elements containing FRT sites used to generate *SK* null mutants are shown as gray triangles, and the breakpoints of the *ΔSK* allele are denoted. The *SK* BAC rescue and *SK* isoforms, *SK-M* and *SK-V*, are schematically shown.

(B) *SK* null mutant animals are hypersensitive to noxious heat (42°C). *ΔSK* larvae (white bar) show hypersensitivity to noxious heat compared to control animals (black bar). Replacing *SK* in the genome with two copies of the BAC transgenes fully rescue the nociception defect (black bar). The *SK* mutant hypersensitivity phenotype is semi-dominant as animals heterozygous for the deletion (gray bars) show quicker responses compared to control animals. One-way ANOVA with Dunnett's test, ***$p < 0.001$, **$p < 0.01$, *$p < 0.05$. Data are presented as mean ± SEM.

(C) Latency to respond to a 42°C probe in *SK* mutant larvae expressing *SK-M* in the class IV neurons (black bar) is significantly different from *ΔSK* larvae (white bars) but not control animals (back bar). Latency to respond to a 42°C probe in *SK* mutant larvae expressing *SK-V* in the class IV neurons (black bar) is significantly different from control larvae (black bar) but not *ΔSK* mutant larvae (white bars). Data are presented as mean ± SEM. One-way ANOVA followed by Tukey's test. ***$p < 0.001$.

(D) Mechanical nociception assay using a 30-mN von Frey fiber. *ΔSK* mutants (white bar) show hypersensitivity to noxious mechanical stimulation compared to control animals (black bar). Replacing *SK* in the genome with two copies of the BAC transgenes rescue the nociception defect (black bar). The *SK* mutant hypersensitivity phenotype is semi-dominant as animals heterozygous for the deletion (gray bars) show hypersensitivity compared to control animals. Fisher's exact test with Holm-Bonferroni correction. Data are presented as percentages ± 95% confidence intervals. *$p < 0.05$.

(E) Expression of SK isoform M in class IV neurons rescues the mechanical nociception phenotype of *SK* mutant. Fisher's exact test with Holm-Bonferroni correction. Data are presented as percentages ± 95% confidence intervals. ***$p < 0.001$.

(F) *ΔSK* mutant animals show normal gentle touch responses. One-way ANOVA with Dunnett's test, $p > 0.05$. Data are presented as mean ± SEM, see Table S2 for sample sizes.

one or two copies of the BAC transgene covering the *SK* genomic region (Figure 2A). The nociception hypersensitivity phenotype was fully reverted in rescue animals containing two copies of the BAC transgene (Figure 2B). Interestingly, animals heterozygous for the *SK* mutation exhibit hypersensitivity to noxious heat but to a lesser degree than homozygotes (4.8 s). Note that testing of heterozygotes can only be performed in female larvae as *SK* is located on the X chromosome (thus, female larvae were used in all experiments to allow for consistent comparisons). One copy of the BAC rescue transgene provides only partial rescue of the hypersensitivity phenotype (5.0 s) but two copies fully rescued (Figure 2B). These data combined support a dosage-sensitive, semi-dominant thermal nociception defect for *SK* mutants that requires two copies of the BAC transgene for phenotypic full rescue.

To test for a nociceptor-specific requirement for *SK*, we expressed the *SK-M* transcript under control of the *ppk-GAL4* driver in the *SK* mutant background (Figure 2A). This manipulation fully rescued the hypersensitive nociception phenotype of the *SK* mutant animals (Figure 2C), confirming the site of action for SK in the nociceptor neurons. SK-M is one of eight long protein isoforms that are annotated on Flybase, and there are an additional six predicted short isoforms (Gramates et al., 2017). As well, we have cloned a cDNA for a transcript encoding a seventh short SK isoform (*SK-V*, Figure 2A). Unlike our experiments with *SK-M*, expression of the *SK-V* transcript in nociceptors did

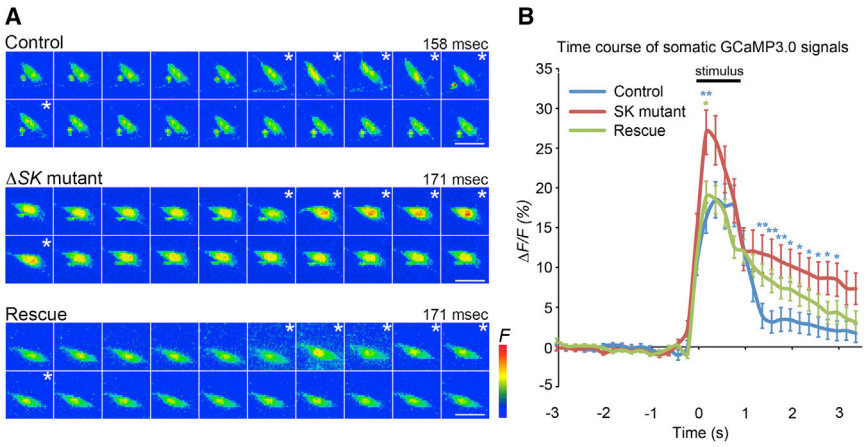

Figure 3. Optical Recordings Show *SK* Mutant Enhances Force-Triggered Ca^{2+} Response of Class IV Neurons

(A) Maximum-intensity projections from Z-stack time series. (Control: upper) Images of representative class IV ddaC neuron expressing GCaMP3.0, displaying increased GCaMP3.0 fluorescence during stimulation with a 50 mN probe (asterisks) (1 frame = 158 ms). (*SK* mutant: middle) Images of representative *SK* mutant ddaC neuron shows higher increase in GCaMP3.0 intensity relative to controls during stimulation (asterisks) (1 frame = 171 ms). (Rescue: bottom) Images of representative ddaC neuron repressing UAS-SK isoform M in *SK* mutant background (1 frame = 171 ms). Scale bars: 10 μm.

(B) Traces showing average peak $\Delta F/F_{0\%}$ of ddaC neurons in each genotype before, during, and after mechanical stimulation. The bar above the trace shows the average length of the mechanical stimulus (0.93 ± 0.02 s). Statistical analysis was performed using a one-way ANOVA with Tukey's HSD post hoc for pairwise comparisons. Data are presented as mean ± SEM. Blue asterisks show control versus *SK* mutant. The green asterisk shows *SK* mutant versus rescue. **p < 0.01 and *p < 0.05 in each time point.

not result in a rescue of the hypersensitive mutant phenotype (Figure 2C). These experiments suggest that long SK isoforms may be more important than short isoforms for suppressing the thermal sensitivity of nociceptors.

SK Negatively Regulates Mechanical Nociception Behavior

The elaborately branched class IV neurons function as polymodal nociceptors, playing a role in both thermal (≥39°C) and mechanical nociception (≥30 mN). Channels expressed in class IV neurons such as such Painless and dTRPA1 are required for both thermal and mechanical nociception, while Pickpocket, Balboa/PPK26, and Piezo have more specific roles in mechanical nociception (Tracey et al., 2003; Zhong et al., 2010, 2012; Neely et al., 2011; Kim et al., 2012; Mauthner et al., 2014; Gorczyca et al., 2014; Guo et al., 2014). Interestingly, *SK* mutant larvae showed enhanced nocifensive responses to a 30-mN mechanical stimulus compared to parental strain animals (Figure 2D). With this stimulus, *ΔSK* mutant animals rolled in response to the noxious force stimuli in 58% of trials, while control animals responded in only 31%. As with thermal nociception, replacing *SK* in the genome by BAC transgene restored the mechanical nociception response to wild-type levels with 38% of BAC rescue animals responding to the 30-mN stimulus (Figure 2D). However, the mechanical nociception phenotype was less sensitive to dosage. Animals heterozygous for the *ΔSK* mutation as well as animals containing one copy of the BAC rescue transgene respond similarly to wild-type animals (44% and 39%, respectively). As with thermal nociception, *UAS-SK-M* expressed under control of the *ppk-GAL4* driver fully rescued the *SK* mutant mechanical nociception phenotype (Figure 2E).

To determine whether SK disruption affects mechanosensation in general, we tested *SK* mutant larvae in an established gentle touch assay (Kernan et al., 1994). Gentle touch responses in *SK* mutants appeared normal (Figure 2F). Thus, the somatosensory effects of SK were more specific to the nociception pathway, regulating nociceptor activity both in response to noxious thermal and mechanical stimuli.

SK Negatively Regulates Nociceptor Excitability

Next, we performed optical recordings from control (Exelixis isogenic *white*) and *SK* mutant larvae expressing the genetically encoded Ca^{2+} indicator, GCaMP3.0 (Tian et al., 2009), under the control of the nociceptor-specific driver, *ppk*-Gal4. In this filleted larval preparation, the md neurons expressing GCaMP3.0 were imaged through the transparent cuticle using high-speed, time-lapse confocal microscopy while stimulated with a 50-mN probe. *ppk-Gal4*-expressing neurons imaged in this preparation showed rapidly increasing GCaMP3.0 signals during the initial application of force and this signal rapidly declined (Figure 3A). In *SK* mutant animals, the peak calcium response (measured at the cell soma) was significantly increased relative to wild-type, and the signal remained elevated above the baseline for several seconds following the mechanical stimulus (Figure 3B). Restoration of SK-M to the mutant background rescued the elevated peak response but did not fully suppress the prolonged signal seen in the mutant (Figure 3B). Thus, although the SK-M isoform can rescue behavioral phenotypes and peak calcium responses in class IV neurons, it is possible that one or more of the 13 other isoforms is required for complete restoration of wild-type responses in this Ca^{2+} imaging assay.

The *SK* Gene Is Expressed in Class IV md Sensory Neurons

To evaluate the expression of *SK*, we examined a transgenic *Drosophila* strain from the *Minos*-mediated integration cassette (MiMIC) collection (Venken et al., 2011). A MiMIC element inserted in the proper orientation into the 5′ non-coding intron of *SK* long isoform transcripts should express EGFP in the native pattern of *SK* (i.e., at endogenous levels in appropriate tissues). We observed EGFP expression in the larval peripheral nervous system in a subset of type I and type II sensory neurons that included the class IV md neurons (Figure 4A). These results reveal that transcripts encoding long-isoform SK proteins are endogenously expressed in the nociceptors and provide additional validation of our tissue-specific *UAS-SK-M* rescue

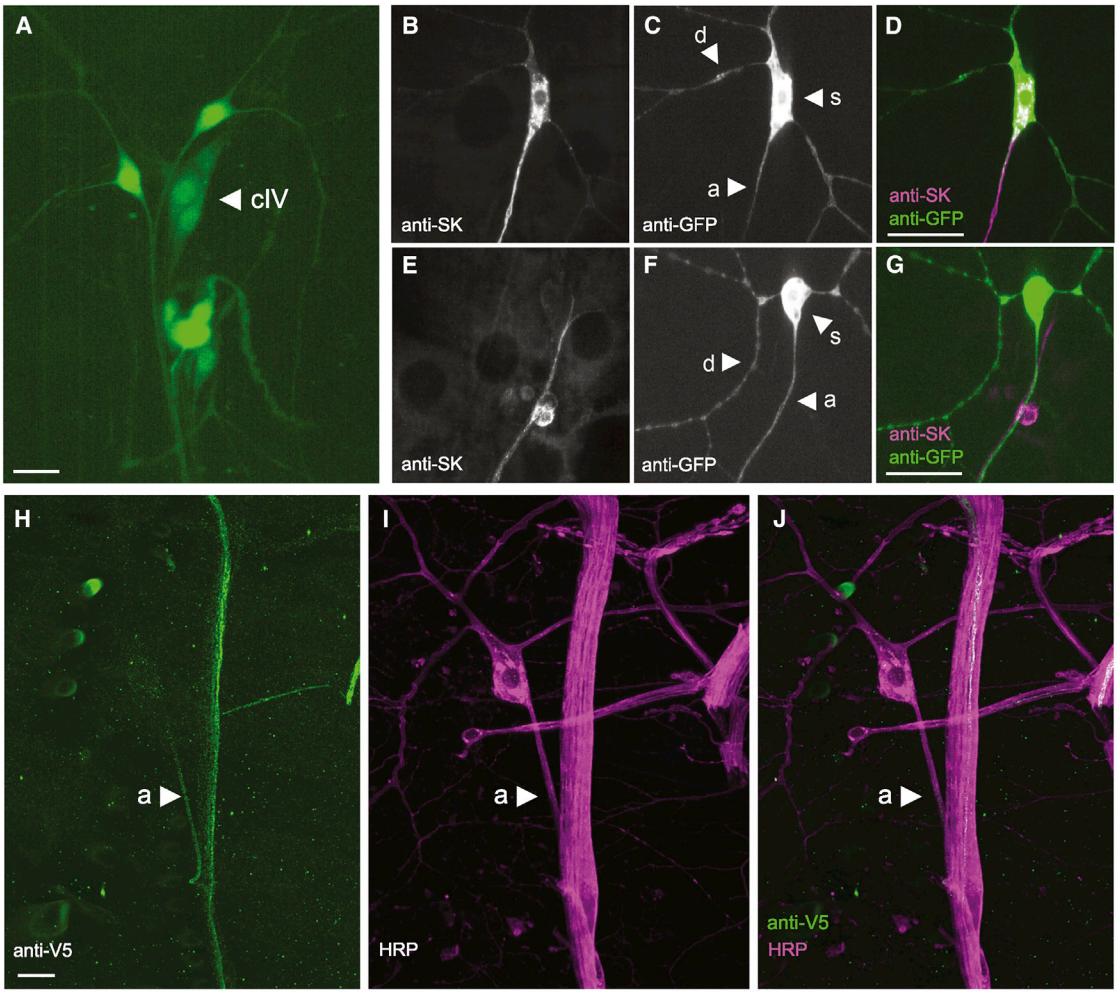

Figure 4. *SK* Is Expressed in Class IV md Neurons and SK::V5 Proteins Localize to the Proximal Axon

Maximum-intensity projection from z-stack images of the dorsal md neuron cluster (segment A4–A6).

(A) A MiMIC element inserted in the 5′ UTR of *SK* expresses GFP in md neurons (arrowhead indicates the class IV neuron ddaC) and es-neurons.

(B–D) Anti-SK antibodies label SK-M proteins expressed in class IV neurons in the *ΔSK* mutant background. SK protein expression (B and magenta in D) and class IV neuron (C and green in D).

(E–G) Endogenous SK protein is detected in axons of sensory neurons in control larvae. SK protein expression (E and magenta in G) and class IV neuron (F and green in G).

(H–J) Anti-V5 antibodies label class IV axons in *SK::V5* larval filet preparation (green; H) that was costained with anti-HRP (magenta; I) and merge of (H) and (I) (J). d, dendrite; s, soma; a, axon. Scale bars: 10 μm.

experiments that restored normal nociception responses to *SK* mutant larvae (Figures 2C and 2E).

SK Proteins Are Localized to a Proximal Compartment of Sensory Axons

The potassium currents mediated by SK channels in mammalian neurons make an important contribution to the afterhyperpolarization (AHP) of action potentials (Faber and Sah, 2002; Pedarzani et al., 2005). However, the precise subcellular function of SK channels is thought to vary depending on the subcellular compartment where it resides. SK proteins have been found in somatic or dendritic compartments in some cell types (reviewed by Rudolph and Thanawala, 2015), and in axons or presynaptic compartments in others (Abou Tayoun et al., 2011). Thus, we wished to identify the subcellular compartment containing SK channels in the nociceptive md neurons.

Using a previously generated anti-SK antibody (Abou Tayoun et al., 2011), we first observed subcellular localization of the SK-M protein used in our nociceptor-specific rescue experiment (Figures 4B–4D). Surprisingly, we found that the rescuing SK-M protein was clearly detectable in the class IV axons and soma (Figures 4B and 4D) but only weakly detectable in proximal dendrites (Figures 4C and 4D). This was consistent with staining in wild-type animals (Figures 4E–4G), where we were able to detect SK protein in axons (Figures 4E and 4G) of sensory neurons but we were unable to detect any expression in the dendrites or soma of class IV neurons (Figures 4F and 4G). Note that, because the SK antibody detects sensory neuron axons of

multiple types in the dorsal sensory neuron cluster, it was often impossible to unambiguously assign the axonal staining observed in wild-type animals to the ddaC class IV axon. However, the anti-SK staining was completely eliminated in null mutant animals confirming specificity of the antibody (Figures S1C–S1E).

These results raised the possibility that SK proteins are required in axons and not in dendrites for nociception. The anti-SK antibody was raised against a purified SK fragment fusion protein largely composed of the N-terminal domain but the exact epitope it detects is not known (Abou Tayoun et al., 2011). Thus, it remained possible that isoforms of SK not detected by this antibody might localize to dendrites. Therefore, in order to detect as many SK protein isoforms as possible, and at their endogenous expression levels, we used clustered regularly interspaced short palindromic repeats (CRISPR)-mediated homologous repair (Gratz et al., 2013; Jinek et al., 2012; Cong et al., 2013) to introduce a V5 epitope tag (Hampel et al., 2011) at the *SK* locus (Figures S2A–S2C). The inserted V5 epitope tag is encoded by an exon present in 13 of the 14 known *SK* transcripts (with the exception of the *SK-J*) located immediately downstream of the sequence encoding the SK calmodulin-binding domain (Figures S2A and S2A′). Interestingly, anti-V5 directed immunofluorescence in animals with our genomic modification was present in the axons of peripheral sensory neurons. Specifically, we observed strong labeling of axons of a subset of type I (external sensory [es] and chordotonal; data not shown) neurons and type II md neurons, including the class IV (Figures 4H–4J). The latter could be unambiguously identified in the v'ada class IV cell because its axon does not bundle with other axons prior to entering the nerve. Interestingly SK::V5 proteins concentrate within a proximal compartment of axons in class IV sensory neurons (Figures 4H and 4J) but were not detected in nociceptor axon terminals in the CNS (Figures S3A–S3C′) or in sensory dendrites of the nociceptive neuron arbor (not shown). The subcellular distribution of SK::V5 proteins along the axon of sensory neurons corroborated labeling of similar neuronal structures with anti-SK antibodies targeting long isoforms of SK (Abou Tayoun et al., 2011) (Figures 4E–4G). Note that the SK-J protein contains the N-terminal domain that was used for raising the anti-SK antibody, making it unlikely that it localizes to dendrites. Thus, our evidence combined suggests SK proteins in axons, and not in dendrites, are important for nociception. As with all antibody staining approaches, we cannot exclude the possibility that SK channels present in dendrites exist but are beneath the limits of detection by this approach.

Our finding on the axonal localization of SK channel proteins is interesting in several respects. First, it suggests that the enhanced Ca^{2+} signals that we observed in nociceptor soma are potentially caused by backpropagation of action potentials rather than a hyperexcitable soma or dendrites. Second, the proximal axonal localization is consistent with recently described evidence that other GFP-tagged *Drosophila* K^+ channels (Shal and Elk) localize to the axon initial segment in the class I md neurons (Jegla et al., 2016). It is possible that SK regulates the AHP of action potentials as in other systems, and this, in turn, regulates firing frequency. It has been proposed that bursts and pauses in firing of the *Drosophila* nociceptor neurons may be necessary for robust nociception responses (Terada et al., 2016). Additionally, an "unconventional spike" that is triggered by a large dendritic calcium transient has been proposed to be important (Terada et al., 2016). Indeed, a recent study also provided evidence that SK channels could regulate firing, because RNAi against SK was found to cause increases in the firing frequency of nociceptive neurons (Onodera et al., 2017). That study proposed that dendritically localized SK channels might respond to a dendritic Ca^{2+} transient. Although our investigation of the localization of the SK channel proteins makes them well positioned to regulate firing of nociceptive neurons, our finding that SK is localized to axons is inconsistent with the hypothesis that SK is directly regulated by dendritic Ca^{2+}. Nevertheless, our comprehensive analysis, including the generation of null mutant alleles, and genomic and tissue-specific rescue experiments, demonstrates a genuine involvement for SK channels in *Drosophila* nociception. Our studies of protein localization by a CRISPR engineered tagged SK channel, and anti-SK staining of an untagged rescuing cDNA suggest that the likely site of action for this important channel resides in the proximal axon segment and not in dendrites. An interesting question for the future will be to investigate whether Seizure and Tiwaz show a similar axonal localization.

STAR★METHODS

Detailed methods are provided in the online version of this paper and include the following:

- KEY RESOURCES TABLE
- CONTACT FOR REAGENT AND RESOURCE SHARING
- EXPERIMENTAL MODEL AND SUBJECT DETAILS
  - Fly Strains
- METHOD DETAILS
  - Molecular Biology
  - CRISPR Gene Tagging
  - Thermal Nociception Assay
  - Mechanical Nociception Assay
  - Gentle Touch Assay
  - Calcium Imaging
  - Immunostaining
  - Confocal Imaging
- QUANTIFICATION AND STATISTICAL ANALYSIS
- DATA AND SOFTWARE AVAILABILITY

SUPPLEMENTAL INFORMATION

Supplemental Information includes three figures and three tables can be found with this article online at https://doi.org/10.1016/j.celrep.2018.08.070.

ACKNOWLEDGMENTS

We thank the Vienna *Drosophila* Resource Center, Transgenic RNAi Project, and the Exelixis Collection at Harvard Medical School (NIH/NIGMS R01-GM084947). Stocks obtained from the Bloomington *Drosophila* Stock Center (NIH P40OD018537) and vectors obtained from the *Drosophila* Genomics Resource Center (NIH 2P40OD010949) were used in this study. We also thank Sarah Sweeney-Howard, Katherine H. Fisher, and Luuli Tran for technical assistance and members of the Tracey laboratory for helpful discussion.

This work was supported by grants from the NIH (5R21DC010222, 5R01GM086458, and 5R01NS054899) (to W.D.T.). K.C.E.W. and J.R. were supported by pre-doctoral fellowships from the National Science Foundation.

AUTHOR CONTRIBUTIONS

Conceptualization, K.C.E.W. and W.D.T.; Methodology, K.C.E.W., S.E.M., and W.D.T.; Investigation, K.C.E.W., S.E.M., A.T., and J.R.; Writing – Original Draft, K.C.E.W., S.E.M., and W.D.T.; Writing – Review and Editing, K.C.E.W., S.E.M., A.T., J.R., and W.D.T.; Visualization, K.C.E.W., S.E.M., A.T., and J.R.; Supervision, S.E.M. and W.D.T.; Funding Acquisition, K.C.E.W., J.R., and W.D.T.

DECLARATION OF INTERESTS

The authors declare no competing interests.

Received: January 25, 2014
Revised: June 11, 2018
Accepted: August 23, 2018
Published: September 18, 2018

REFERENCES

Abou Tayoun, A.N., Li, X., Chu, B., Hardie, R.C., Juusola, M., and Dolph, P.J. (2011). The *Drosophila* SK channel (dSK) contributes to photoreceptor performance by mediating sensitivity control at the first visual network. J. Neurosci. *31*, 13897–13910.

Abou Tayoun, A.N., Pikielny, C., and Dolph, P.J. (2012). Roles of the *Drosophila* SK channel (dSK) in courtship memory. PLoS One *7*, e34665.

Adelman, J.P., Maylie, J., and Sah, P. (2012). Small-conductance Ca^{2+}-activated K^+ channels: form and function. Annu. Rev. Physiol. *74*, 245–269.

Ainsley, J.A., Pettus, J.M., Bosenko, D., Gerstein, C.E., Zinkevich, N., Anderson, M.G., Adams, C.M., Welsh, M.J., and Johnson, W.A. (2003). Enhanced locomotion caused by loss of the *Drosophila* DEG/ENaC protein Pickpocket1. Curr. Biol. *13*, 1557–1563.

Brand, A.H., and Perrimon, N. (1993). Targeted gene expression as a means of altering cell fates and generating dominant phenotypes. Development *118*, 401–415.

Cong, L., Ran, F.A., Cox, D., Lin, S., Barretto, R., Habib, N., Hsu, P.D., Wu, X., Jiang, W., Marraffini, L.A., and Zhang, F. (2013). Multiplex genome engineering using CRISPR/Cas systems. Science *339*, 819–823.

Dietzl, G., Chen, D., Schnorrer, F., Su, K.C., Barinova, Y., Fellner, M., Gasser, B., Kinsey, K., Oppel, S., Scheiblauer, S., et al. (2007). A genome-wide transgenic RNAi library for conditional gene inactivation in *Drosophila*. Nature *448*, 151–156.

Dubin, A.E., and Patapoutian, A. (2010). Nociceptors: the sensors of the pain pathway. J. Clin. Invest. *120*, 3760–3772.

Faber, E.S., and Sah, P. (2002). Physiological role of calcium-activated potassium currents in the rat lateral amygdala. J. Neurosci. *22*, 1618–1628.

Gao, F.B., Brenman, J.E., Jan, L.Y., and Jan, Y.N. (1999). Genes regulating dendritic outgrowth, branching, and routing in *Drosophila*. Genes Dev. *13*, 2549–2561.

Gertner, D.M., Desai, S., and Lnenicka, G.A. (2014). Synaptic excitation is regulated by the postsynaptic dSK channel at the *Drosophila* larval NMJ. J. Neurophysiol. *111*, 2533–2543.

Gorczyca, D.A., Younger, S., Meltzer, S., Kim, S.E., Cheng, L., Song, W., Lee, H.Y., Jan, L.Y., and Jan, Y.N. (2014). Identification of Ppk26, a DEG/ENaC channel functioning with Ppk1 in a mutually dependent manner to guide locomotion behavior in *Drosophila*. Cell Rep. *9*, 1446–1458.

Gramates, L.S., et al.; the FlyBase Consortium (2017). FlyBase at 25: looking to the future. Nucleic Acids Res. *45*, D663–D671.

Gratz, S.J., Cummings, A.M., Nguyen, J.N., Hamm, D.C., Donohue, L.K., Harrison, M.M., Wildonger, J., and O'Connor-Giles, K.M. (2013). Genome engineering of *Drosophila* with the CRISPR RNA-guided Cas9 nuclease. Genetics *194*, 1029–1035.

Guo, Y., Wang, Y., Wang, Q., and Wang, Z. (2014). The role of PPK26 in *Drosophila* larval mechanical nociception. Cell Rep. *9*, 1183–1190.

Hampel, S., Chung, P., McKellar, C.E., Hall, D., Looger, L.L., and Simpson, J.H. (2011). *Drosophila* Brainbow: a recombinase-based fluorescence labeling technique to subdivide neural expression patterns. Nat. Methods *8*, 253–259.

Honjo, K., Robertson, J., and Tracey, W.D. (2014). Nociception. In Behavioral Genetics of the Fly (Drosophila melanogaster), J. Dubnau, ed. (Cambridge University Press), pp. 66–76.

Honjo, K., Mauthner, S.E., Wang, Y., Skene, J.H.P., and Tracey, W.D., Jr. (2016). Nociceptor-enriched genes required for normal thermal nociception. Cell Rep. *16*, 295–303.

Hu, C., Petersen, M., Hoyer, N., Spitzweck, B., Tenedini, F., Wang, D., Gruschka, A., Burchardt, L.S., Szpotowicz, E., Schweizer, M., et al. (2017). Sensory integration and neuromodulatory feedback facilitate *Drosophila* mechanonociceptive behavior. Nat. Neurosci. *20*, 1085–1095.

Hwang, R.Y., Zhong, L., Xu, Y., Johnson, T., Zhang, F., Deisseroth, K., and Tracey, W.D. (2007). Nociceptive neurons protect *Drosophila* larvae from parasitoid wasps. Curr. Biol. *17*, 2105–2116.

Jackson, F.R., Wilson, S.D., Strichartz, G.R., and Hall, L.M. (1984). Two types of mutants affecting voltage-sensitive sodium channels in *Drosophila melanogaster*. Nature *308*, 189–191.

Jegla, T., Nguyen, M.M., Feng, C., Goetschius, D.J., Luna, E., van Rossum, D.B., Kamel, B., Pisupati, A., Milner, E.S., and Rolls, M.M. (2016). Bilaterian giant ankyrins have a common evolutionary origin and play a conserved role in patterning the axon initial segment. PLoS Genet. *12*, e1006457.

Jinek, M., Chylinski, K., Fonfara, I., Hauer, M., Doudna, J.A., and Charpentier, E. (2012). A programmable dual-RNA-guided DNA endonuclease in adaptive bacterial immunity. Science *337*, 816–821.

Kernan, M., Cowan, D., and Zuker, C. (1994). Genetic dissection of mechanosensory transduction: mechanoreception-defective mutations of Drosophila. Neuron *12*, 1195–1206.

Kim, S.E., Coste, B., Chadha, A., Cook, B., and Patapoutian, A. (2012). The role of *Drosophila* Piezo in mechanical nociception. Nature *483*, 209–212.

Köhler, M., Hirschberg, B., Bond, C.T., Kinzie, J.M., Marrion, N.V., Maylie, J., and Adelman, J.P. (1996). Small-conductance, calcium-activated potassium channels from mammalian brain. Science *273*, 1709–1714.

Mauthner, S.E., Hwang, R.Y., Lewis, A.H., Xiao, Q., Tsubouchi, A., Wang, Y., Honjo, K., Skene, J.H., Grandl, J., and Tracey, W.D., Jr. (2014). Balboa binds to pickpocket in vivo and is required for mechanical nociception in *Drosophila* larvae. Curr. Biol. *24*, 2920–2925.

Neely, G.G., Keene, A.C., Duchek, P., Chang, E.C., Wang, Q.P., Aksoy, Y.A., Rosenzweig, M., Costigan, M., Woolf, C.J., Garrity, P.A., and Penninger, J.M. (2011). TrpA1 regulates thermal nociception in *Drosophila*. PLoS One *6*, e24343.

Ni, J.Q., Liu, L.P., Binari, R., Hardy, R., Shim, H.S., Cavallaro, A., Booker, M., Pfeiffer, B.D., Markstein, M., Wang, H., et al. (2009). A *Drosophila* resource of transgenic RNAi lines for neurogenetics. Genetics *182*, 1089–1100.

Onodera, K., Baba, S., Murakami, A., Uemura, T., and Usui, T. (2017). Small conductance Ca^{2+}-activated K^+ channels induce the firing pause periods during the activation of *Drosophila* nociceptive neurons. eLife *6*, e29754.

Pagadala, P., Park, C.K., Bang, S., Xu, Z.Z., Xie, R.G., Liu, T., Han, B.X., Tracey, W.D., Jr., Wang, F., and Ji, R.R. (2013). Loss of NR1 subunit of NMDARs in primary sensory neurons leads to hyperexcitability and pain hypersensitivity: involvement of Ca^{2+}-activated small conductance potassium channels. J. Neurosci. *33*, 13425–13430.

Parks, A.L., Cook, K.R., Belvin, M., Dompe, N.A., Fawcett, R., Huppert, K., Tan, L.R., Winter, C.G., Bogart, K.P., Deal, J.E., et al. (2004). Systematic generation of high-resolution deletion coverage of the *Drosophila melanogaster* genome. Nat. Genet. *36*, 288–292.

Pedarzani, P., McCutcheon, J.E., Rogge, G., Jensen, B.S., Christophersen, P., Hougaard, C., Strøbaek, D., and Stocker, M. (2005). Specific enhancement of

SK channel activity selectively potentiates the afterhyperpolarizing current I(AHP) and modulates the firing properties of hippocampal pyramidal neurons. J. Biol. Chem. *280*, 41404–41411.

Ritter, A.M., and Mendell, L.M. (1992). Somal membrane properties of physiologically identified sensory neurons in the rat: effects of nerve growth factor. J. Neurophysiol. *68*, 2033–2041.

Rudolph, S., and Thanawala, M.S. (2015). Location matters: somatic and dendritic SK channels answer to distinct calcium signals. J. Neurophysiol. *114*, 1–5.

Terada, S., Matsubara, D., Onodera, K., Matsuzaki, M., Uemura, T., and Usui, T. (2016). Neuronal processing of noxious thermal stimuli mediated by dendritic Ca^{2+} influx in *Drosophila* somatosensory neurons. eLife *5*, e12959.

Thibault, S.T., Singer, M.A., Miyazaki, W.Y., Milash, B., Dompe, N.A., Singh, C.M., Buchholz, R., Demsky, M., Fawcett, R., Francis-Lang, H.L., et al. (2004). A complementary transposon tool kit for *Drosophila melanogaster* using P and piggyBac. Nat. Genet. *36*, 283–287.

Tian, L., Hires, S.A., Mao, T., Huber, D., Chiappe, M.E., Chalasani, S.H., Petreanu, L., Akerboom, J., McKinney, S.A., Schreiter, E.R., et al. (2009). Imaging neural activity in worms, flies and mice with improved GCaMP calcium indicators. Nat. Methods *6*, 875–881.

Tracey, W.D., Jr., Wilson, R.I., Laurent, G., and Benzer, S. (2003). *painless*, a *Drosophila* gene essential for nociception. Cell *113*, 261–273.

Tsubouchi, A., Caldwell, J.C., and Tracey, W.D. (2012). Dendritic filopodia, Ripped Pocket, NOMPC, and NMDARs contribute to the sense of touch in *Drosophila* larvae. Curr. Biol. *22*, 2124–2134.

Venken, K.J., He, Y., Hoskins, R.A., and Bellen, H.J. (2006). P[acman]: a BAC transgenic platform for targeted insertion of large DNA fragments in *D. melanogaster*. Science *314*, 1747–1751.

Venken, K.J.T., Carlson, J.W., Schulze, K.L., Pan, H., He, Y., Spokony, R., Wan, K.H., Koriabine, M., de Jong, P.J., White, K.P., et al. (2009). Versatile P[acman] BAC libraries for transgenesis studies in *Drosophila melanogaster*. Nat. Methods *6*, 431–434.

Venken, K.J.T., Schulze, K.L., Haelterman, N.A., Pan, H., He, Y., Evans-Holm, M., Carlson, J.W., Levis, R.W., Spradling, A.C., Hoskins, R.A., and Bellen, H.J. (2011). MiMIC: a highly versatile transposon insertion resource for engineering *Drosophila melanogaster* genes. Nat. Methods *8*, 737–743.

Williams, M.J., Goergen, P., Rajendran, J., Klockars, A., Kasagiannis, A., Fredriksson, R., and Schiöth, H.B. (2014). Regulation of aggression by obesity-linked genes *TfAP-2* and *Twz* through octopamine signaling in *Drosophila*. Genetics *196*, 349–362.

Xiang, Y., Yuan, Q., Vogt, N., Looger, L.L., Jan, L.Y., and Jan, Y.N. (2010). Light-avoidance-mediating photoreceptors tile the *Drosophila* larval body wall. Nature *468*, 921–926.

Zhong, L., Hwang, R.Y., and Tracey, W.D. (2010). Pickpocket is a DEG/ENaC protein required for mechanical nociception in *Drosophila* larvae. Curr. Biol. *20*, 429–434.

Zhong, L., Bellemer, A., Yan, H., Ken, H., Jessica, R., Hwang, R.Y., Pitt, G.S., and Tracey, W.D. (2012). Thermosensory and nonthermosensory isoforms of *Drosophila melanogaster* TRPA1 reveal heat-sensor domains of a thermoTRP channel. Cell Rep. *1*, 43–55.

STAR★METHODS

KEY RESOURCES TABLE

REAGENT or RESOURCE	SOURCE	IDENTIFIER
Antibodies		
Rabbit anti-dSK (polyclonal antibody targeting SK's N-terminal domain)	Patrick Dolph (Abou Tayoun et al., 2011)	N/A
Mouse anti-V5	Thermo Fisher Scientific	Cat# R960-25;RRID:AB_2556564
Rabbit anti-GFP	Thermo Fisher Scientific	Cat# A-11122;RRID:AB_221569
Rabbit anti-HRP	Jackson ImmunoResearch Laboratories	Cat# 323-005-021;RRID:AB_2314648
Alexa Fluor. 488 goat anti-mouse	Thermo Fisher Scientific	Cat# A-11029;RRID:AB_2534088
Alexa Fluor. 488 goat anti-rabbit	Thermo Fisher Scientific	Cat# A-11034;RRID:AB_2576217
		Cat# A-11008;RRID:AB_143165
Alexa Fluor. 546 goat anti-mouse	Thermo Fisher Scientific	Cat# A-11030;RRID:AB_2534089
Alexa Fluor. 546 goat anti-rabbit	Thermo Fisher Scientific	Cat# A-11035;RRID:AB_2534093
Deposited Data		
SK-V isoform sequence	GenBank	MH001552
Experimental Models: Organisms/Strains		
D. melanogaster: RNAi strains targeting K^+ channels (See Table S1)	Vienna Drosophila Resource Center; Bloomington Drosophila Stock Center	See Table S1
D. melanogaster: y^1 *w*; md-GAL4 (aka* $GAL4^{109(2)80}$*)*	Bloomington Drosophila Stock Center	BDSC: 8769; FlyBase: FBti0015554
D. melanogaster: y^1 *w*; md-GAL4 (aka* $GAL4^{109(2)80}$*)*	Bloomington Drosophila Stock Center	BDSC: 8769; FlyBase: FBti0015554
D. melanogaster: w; ppk-GAL4 (aka ppk1.9-GAL4)*	Ainsley et al., 2003	FlyBase: FBal0152201
D. melanogaster: w^{1118}*; UAS-Dicer2*	Vienna Drosophila Resource Center	60009
D. melanogaster: w;; $UAS\text{-}GCaMP3.0^{attp2}$	Bloomington Drosophila Stock Center	BDSC: 32236
D. melanogaster: y^1 w^{67c23}*;; attp2*	Bloomington Drosophila Stock Center	BDSC: 8622; FlyBase: FBti0040535
*D. melanogaster: w** $P\{XP\}^{d01963}$	The Exelixis Collection at the Harvard Medical School	*d01963;* FlyBase: FBti0054688
D. melanogaster: w pBac{WH}*SK^{f01403}	The Exelixis Collection at the Harvard Medical School	f01403; FlyBase: FBst1016953
D. melanogaster: w^{1118} *ΔSK*	Generated in this study	N/A
D. melanogaster: w^{1118} *SK::V5*	Generated in this study	N/A
D. melanogaster: w^{1118} *; UAS-SK-M*	Generated in this study	N/A
D. melanogaster: w^{1118} *; UAS-SK-V*	Generated in this study	N/A
Oligonucleotides		
See Table S3	N/A	N/A
Recombinant DNA		
BAC: *CH321-90C05* (aka *CHORI-321-90C05*)	BACPAC Resources Center (BPRC)	CH321-90C05
TOPO-XL	Thermo Fisher Scientific	Cat# K8050
pENTR (Gateway Entry Vector)	Thermo Fisher Scientific	Cat# K240020
pTW (*Drosophila* Gateway Vector Collection)	Drosophila Genomics Resource Center	Gateway Collection

CONTACT FOR REAGENT AND RESOURCE SHARING

Further information and requests for resources and reagents should be directed to and will be fulfilled by the Lead Contact, W. Dan Tracey (dtracey@indiana.edu).

EXPERIMENTAL MODEL AND SUBJECT DETAILS

Fly Strains

All fly strains used in this study are detailed in Key Resources Table and Table S1. We identified K^+ channel genes using the controlled vocabulary function at FlyBase (http://flybase.org/) for all genes with K^+ channel activity (http://flybase.org/cgi-bin/cvreport.html?id=GO:0005267). We used these fly strains: *w; md-Gal4;UAS-Dicer2* (primary screen), *w; ppk-Gal4;UAS-Dicer2* (secondary screen), and *w; ppk-Gal4 UAS-GCaMP3.0*. Fly stocks with UAS lines and TRiP RNAi lines were provided by the Bloomington Stock Center. RNAi lines for screening were provided by the Vienna *Drosophila* RNAi Center (Dietzl et al., 2007). *Drosophila* stocks were raised on standard cornmeal molasses fly food medium at 25°C. Where possible, we used balancers containing the *Tb* marker so that the inheritance of the UAS insertion(s) could be followed. Exelixis lines, $P\{XP\}^{d01963}$ and $pBAC\{WH\}SK^{f01403}$, were provided by the Exelixis collection at Harvard Medical School (Thibault et al., 2004) and used to generate FLP-FRT mediated *SK* mutant flies (crossing strategy outlined in (Parks et al., 2004)). *SK* genomic rescue strains were generated by injection of BAC CH321-90C05 (Venken et al., 2009) performed by Rainbow Transgenic Flies, Inc. for *PhiC31*-mediated chromosome integration into the *attP2* docking site. Transgenic flies containing the BAC rescue construct were crossed into *SK* deletion background to generate the genomic rescue strain. BestGene, Inc. performed microinjections of pUAST-SK-M and pUAST-SK-V vectors into w^{1118} and transgenic flies were generated via standard P-element mediated transformation.

METHOD DETAILS

Molecular Biology

To preliminarily screen for deletion of *SK*, polymerase chain reaction (PCR) was performed on genomic DNA extracted from wandering third-instar larvae with the putative FLP/FRT-mediated *SK* deletion. The QIAGEN DNeasy® Blood and Tissue kit was used for DNA extraction and the forward primer: 5′-ATGTCAATTCAGAAGCTTAACGACAC-3′ and the reverse primer: 5′- TGCAGTTGCTGCT GATGCAGAT-3′ were used to test for absence of *SK* gene product by PCR amplification (primer pair 2, Figures S1A and S1B). Three additional primer pairs were used to confirm the *SK* deletion. From the upstream gene, *CanB*, into the *p{XP}* element: forward primer 5′-GCAGTCGTGTATTTGCTGTCG-3′ and reverse primer 5′-TACTATTCCTTTCACTCGCACTTATTG-3′ (primer pair 1, Figures S1A and S1B). From within the *SK* locus: forward primer 5′-TTATTCATGATAGATAACTGCGCTGACG-3′ and reverse primer 5′-CAC CATGCCGCAGGTGAGGGTGATA-3′ (primer pair 3, Figures S1A and S1B). From the *pBac{WH}* into C-terminal end of *SK*: forward primer 5′-CCTCGATATACAGACCGATAAAAC-3′ and reverse primer 5′-ATCCTGGTGCCCTACGATCTATGT-3′ (primer pair 4, Figures S1A and S1B). Lastly, control primers targeting Caα1D, forward primer: 5′-CAACCGGATGTGAAGTGCG-3′ and the reverse primer: 5′-CTTGGCACTT CGCCTGAAGG-3′, were used to confirm integrity of DNA preps (control primer pair, Figure S1B).

For the cloning of *SK-M* and *SK-V* rescue constructs, RT-PCR was performed on total RNA extracts (TRIzol, Life Technologies) from Canton-S third instar larvae. The SuperScript III reverse transcriptase enzyme (Life Technologies) and Oligo$(dT)_{12\text{-}18}$ primer (Life Technologies) were used to direct the synthesis of first strand cDNA. For *SK-M* and *SK-V* cDNA amplification, PCR was performed using the reverse primer 5′- TCAGCTAGAATGTGGAAACAGCAT-3′, and either the forward primer 5′-ATGTCAATTCA GAAGCTTAACGAC-3′ to target the *SK-M* isoform or the forward primer 5′- ATGTCGCCGGCCTTCTGC-3′ to target the *SK-V* isoform. The *SK-M* and *SK-V* PCR products were subsequently cloned into the TOPO-XL vector (Life Technologies) and fully sequenced. The complete sequence for the newly cloned *SK-V* isoform was deposited in GenBank (accession number MH001552). The following primers were used to target the desired *SK-M* and *SK-V* amplicons for subcloning into the pENTR/D-TOPO vector (Thermo Fisher Scientific): 5′-CACCATGTCAATTCAGAAGCTTAACGAC-3′ and 5′-TCAGCTAGAATGTGGAAACAG CATG-3′ for *SK-M*, or 5′-CACCATGTCGCCGGCCTTCT-3′ and 5′- TCAGCTAGAATGTGGAAACAGCATGGGC-3′ for *SK-V*. Gateway recombination technology was used to further subclone the *SK-M* and *SK-V* cDNAs from pENTR into the final pTW destination vector (i.e., *pUASt-SK-M* and *pUASt-SK-V)* via the LR Clonase enzyme (Life Technologies).

CRISPR Gene Tagging

A V5 epitope tag was introduced at the SK locus (Figures S2A, S2A′, and S2B) using a single-stranded oligodeoxynucleotide (ssODN) homology directed repair CRISPR-Cas9 approach (Gratz et al., 2013). The guide RNA sequence 5′-CCATTCAAGCGC CAACGCCC-3′ was cloned into the BbsI site of pU6-BbsI-chiRNA plasmid (Gratz et al., 2013) and co-injected at a concentration of 250 ng/μL with the ssODN donor repair template 5′- GAGCGGATCGAGCAGCGGCGGAAC TTTTTACATCCTGACACAGCTG CAGTTGCCCCCATTGGTAAGCCTATCCCTAACCCTCTCCTCGG**TCTAGA**TTCTACGCAAGCGCCAACGCCCCAATCGATGTTCA ATGCAGCGCCCATGCTGTTTCCACATTCTAGG-3′ (Integrated DNA Technologies) at a concentration of 100ng/uL into w^{1118};; $PBac\{vas\text{-}Cas9\}^{VK00027}$ embryos. Underlined sequence in the ssODN repair template indicates the introduced in-frame V5 epitope tag with a diagnostic XbaI restriction site (bold text). F_0 flies were crossed to w^{1118} flies and single F_1 founders were mated with an FM7c balancer strain to establish independent lines. To screen for V5 integrations events, PCR and Xba1 RFLP analysis were conducted on genomic DNA extracted from individual F_1 candidate flies. PCR was performed with the following primer pair: 5′-GAGCGTTTAACCAACCTAGAG-3′ and 5′-GCAGTTAGTGTTCGTCCAAAG-3′. PCR amplified products showing the desired XbaI cleavage were selected for further sequence verification of proper in-frame *SK::V5* integration (Figure S2B). Candidate strains were sequenced both in genomic DNA and cDNA (Figure S2C).

Thermal Nociception Assay

Thermal nociception assays were as described previously (Honjo et al., 2014, 2016). In a primary screen, approximately 10–20 lines were tested per day and each day included a control cross for the driver line to the relevant isogenic background (*md-Gal4/+;UAS-Dicer 2/+*). We assigned alternative numeric labels to the VDRC lines so that the identity of the genes was blind to the tester throughout the entire screening process. The gene candidates were decoded following completion of the screen. Five to fifteen larvae were tested in the initial screen and an average latency was calculated. *UAS-IR* lines were selected for retesting if they displayed a latency that was one or more standard deviation from the control strain mean (*w; md-Gal4/+;UAS-Dicer2/+*, *w; ppk-Gal4/+;UAS-Dicer2/+*). We re-tested approximately 20-40 larvae for each line kept after the initial screen. For *SK* genetic mutant testing and rescue experiments, only female wandering, third-instar larvae were tested to measure dosage sensitivity.

Mechanical Nociception Assay

Crosses were prepared as with the thermal nociception assay. Wandering, third-instar larvae were collected between days five and seven, and stimulated with calibrated (~30–50 mN) von Frey fibers as previously described (Hwang et al., 2007; Zhong et al., 2010; Mauthner et al., 2014). Noxious mechanical stimuli were delivered by the rapid depression and release of the fiber so that the fiber would begin to bend on the dorsal surface of the larva. The stimulus was delivered between abdominal segments four, five, and six. The percent response following the stimulus was calculated for each genotype. For *SK* genetic mutant testing and rescue experiments, only female wandering, third-instar larvae were tested to measure dosage sensitivity.

Gentle Touch Assay

The gentle touch behavioral assay was performed as previously described (Kernan et al., 1994; Tsubouchi et al., 2012). For *SK* genetic mutant testing and rescue experiments, only female wandering, third-instar larvae were tested to measure dosage sensitivity.

Calcium Imaging

Calcium imaging experiments were performed as described previously (Tsubouchi et al., 2012) but with a 50 mN probe.

Immunostaining

The anti-SK was kindly provided by the Dolph lab (Abou Tayoun et al., 2011). The anti-SK antibody was used at a concentration of 1:2000, mouse anti-V5 antibody (Thermo Fisher Scientific) was used at a concentration of 1:200, anti-GFP antibody was used at a concentration of 1:250 (Thermo Fisher Scientific), and an anti-HRP antibody was used at concentration of 1:100 (Jackson ImmunoResearch Lab). All secondary antibodies were used at a concentration of 1:600 or 1:1000 (Alexa Flours from Thermo Fisher Scientific). Detailed staining protocols are available upon request.

Confocal Imaging

For live GFP imaging, larvae were anesthetized and mounted as previously described in (Mauthner et al., 2014). Confocal Z stacks of the dorsal cluster from the SK^{MI1037} MiMIC line were taken on a Zeiss LSM 5 LIVE. For immunostained tissue, anti-SK images were taken on a LSM 5 LIVE confocal microscope using a 40X objective and anti-V5 images were taken on an LSM 880 63x objective.

QUANTIFICATION AND STATISTICAL ANALYSIS

The following statistical analyses were used in this study: Fisher's Exact test with Holm-Bonferroni correction for nonparametric data analysis, Student's t test for comparing two means, one-way ANOVA with post hoc Tukey's HSD test for multiple comparisons of parametric data, or one-way ANOVA with Dunnett's test for comparisons of parametric data. All statistical analyses were performed using Graphpad, Prism, or R and are specified in the figure legends (including p value significance thresholds). The larval sample sizes for the behavioral assays are noted in Table S2 or in STAR Methods. Error bars denoting standard error of the mean or confidence intervals are also indicated in relevant figure legend

DATA AND SOFTWARE AVAILABILITY

The accession number for the *SK-V* isoform sequence reported in this paper is GenBank: MH001552.

Cell Reports, Volume *24*

Supplemental Information

The *Drosophila* Small Conductance Calcium-Activated Potassium Channel Negatively Regulates Nociception

Kia C.E. Walcott, Stephanie E. Mauthner, Asako Tsubouchi, Jessica Robertson, and W. Daniel Tracey

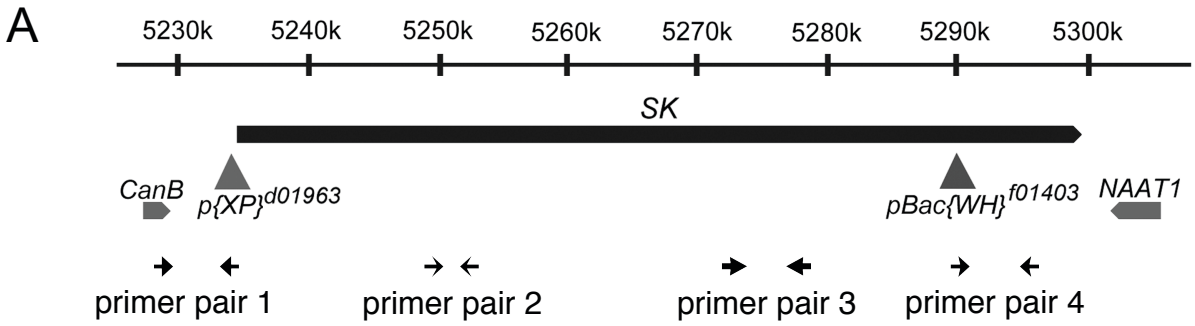

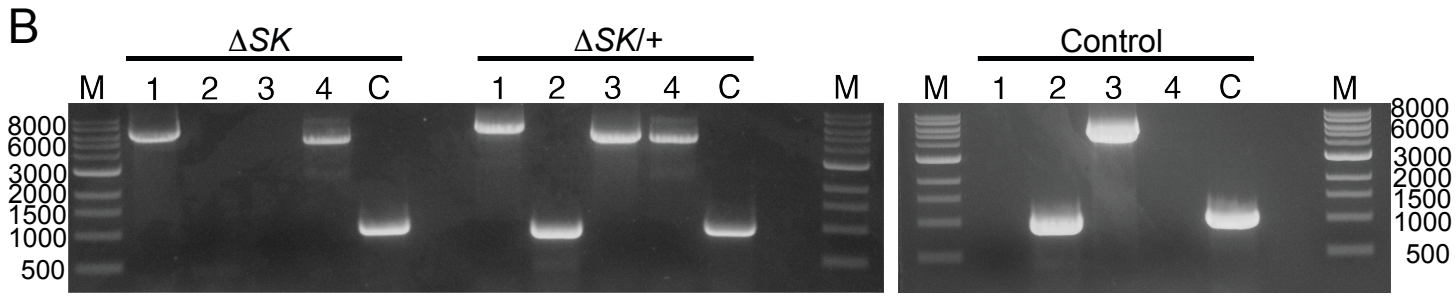

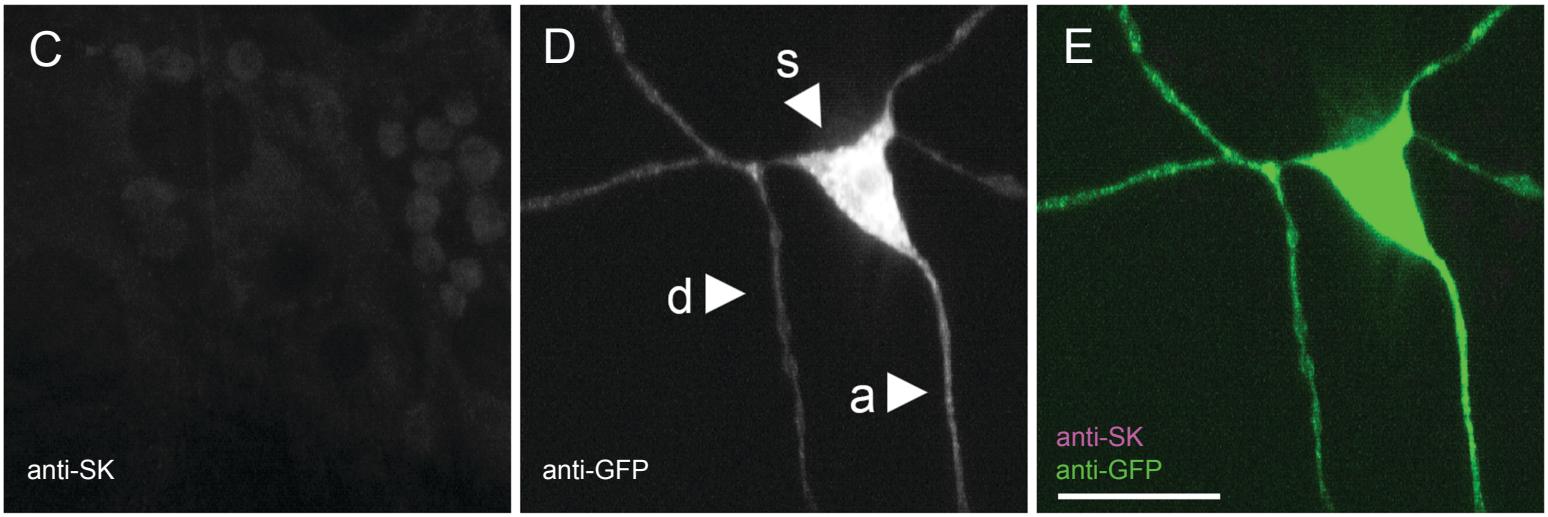

Figure S1. Confirmation of *SK* deletion by PCR and immunostainting. Related to Figure 2.
(A) Arrowheads indicate the *P{XP}*^{d01963} and *pBac{WH}SK*^{f01403} transposable elements used to generate the FLP-FRT mediated *SK* deletion (*ΔSK*). The arrows numbered 1 - 4 represent distinct primer pairs for PCR confirmation of the *SK* deletion (primer set 1: 7.6kb, primer set 2: 900bp, primer set 3: 5.3kb, primer set 4: 5.8kb). **(B)** Agarose gel electrophoresis of PCR amplified products using primer pairs 1 and 4 that flank the *SK* deletion, and *SK*-specific primer pairs 2 and 3. Lane M is the NEB 1 kb DNA ladder. The *ΔSK* transgenic animals show amplified products for primer set 1 and 4 and do not show a product for the *SK*-specific primer pairs set 2 and 3. Transgenic animals heterozygous for the *SK* deletion (*ΔSK*/+) show products for all primer pairs as they have one copy of the WT and mutant chromosome each. Control transgenic animals (isogenic *white*) do not show products for primer set 1 and 4; they do not contain the transposable elements in their genome. Control primers against *Caα 1D* (1kb) demonstrate integrity of the genomic DNA preps. All transgenic animals used for PCR analysis were virgin females (n>5). **(C-E)** Maximum intensity projection from z-stack confocal micrographs representative of the dorsal md neuron cluster (abdominal segment A4-A6) in larvae. Endogenous SK proteins are not at detectable levels in sensory neurons of *SK* null mutant larvae when immunostaining with anti-SK antibodies targeting the long isoform. SK protein expression (C and magenta in E) and class IV neuron (D and green in E) labeling. Scale bar is 10μm.

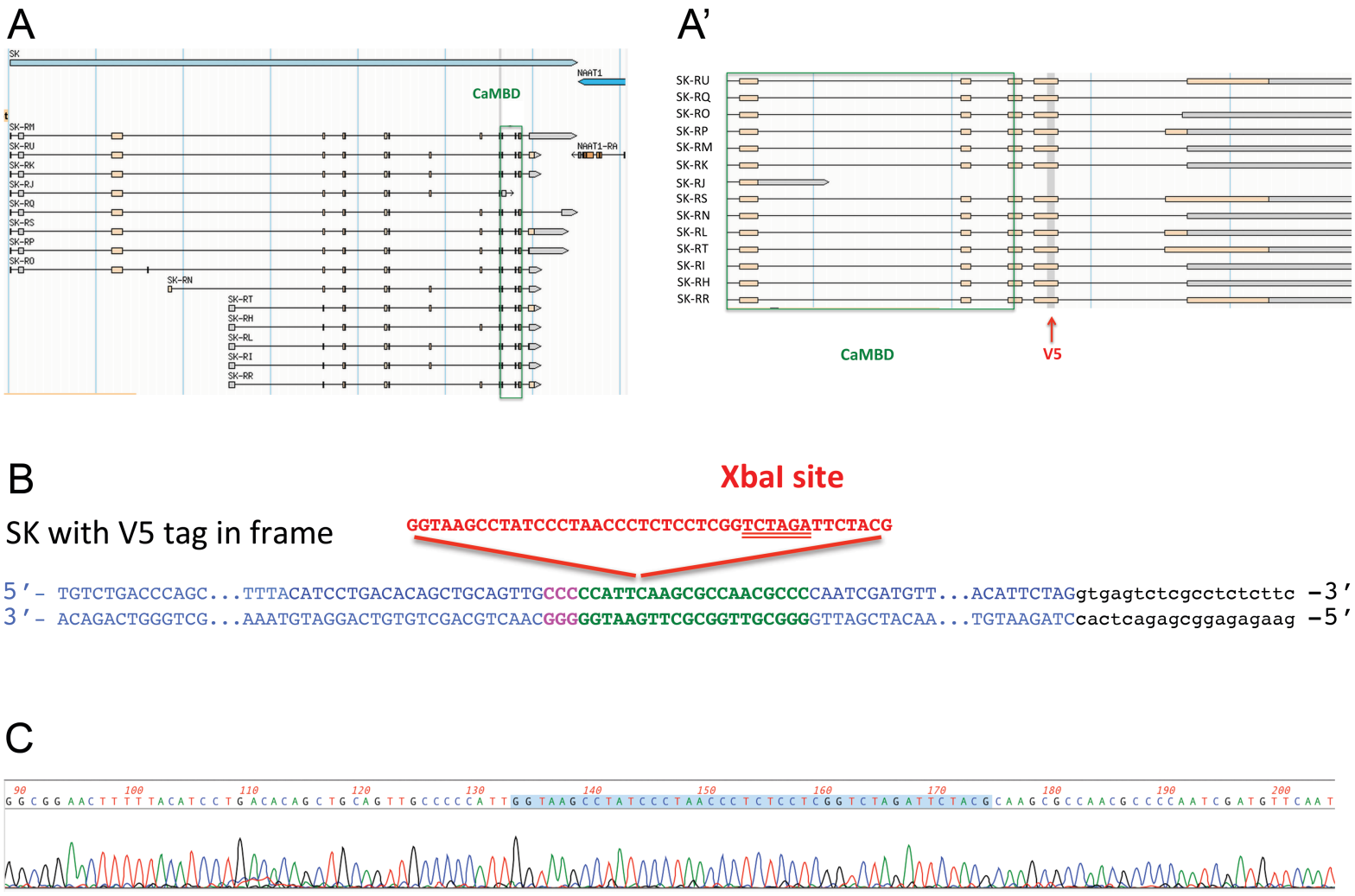

Figure S2. CRISPR engineered *V5* epitope at *SK* locus. Related to Figure 4.
(A) Image of *SK* gene structure and predicted/known *SK* transcripts taken from the Flybase Genome Browser version FB2017_04, released August 22, 2017 (Gramates et al., 2017). The exons encoding the calmodulin-binding domain (CaMBD) in 13 out of the 14 predicted *SK* transcripts are boxed in green. **(A')** Zoomed in view of the *SK* locus shows the in-frame *V5* epitope tag (red arrow) that was engineered downstream of the CaMBD using an ssODN template (shaded grey region) for CRISPR mediated homologous repair. Predicted transcripts are indicated and the *V5* tag was inserted within last common exon after the CaMBD. **(B)** Predicted sequence of the in frame *V5* tag (red sequence) contains an XbaI restriction site (double underlined red sequence) for PCR-RFLP analysis. Exon sequence in black, intron sequence in blue, gRNA sequence in green, and PAM site in magenta. **(C)** Sanger sequencing results show precise insertion of V5 tag. Sequences are from cloned cDNA (generated by reverse transcription and amplified via PCR) targeting *SK* transcripts that span the *V5* insertion and flank exon splice sites.

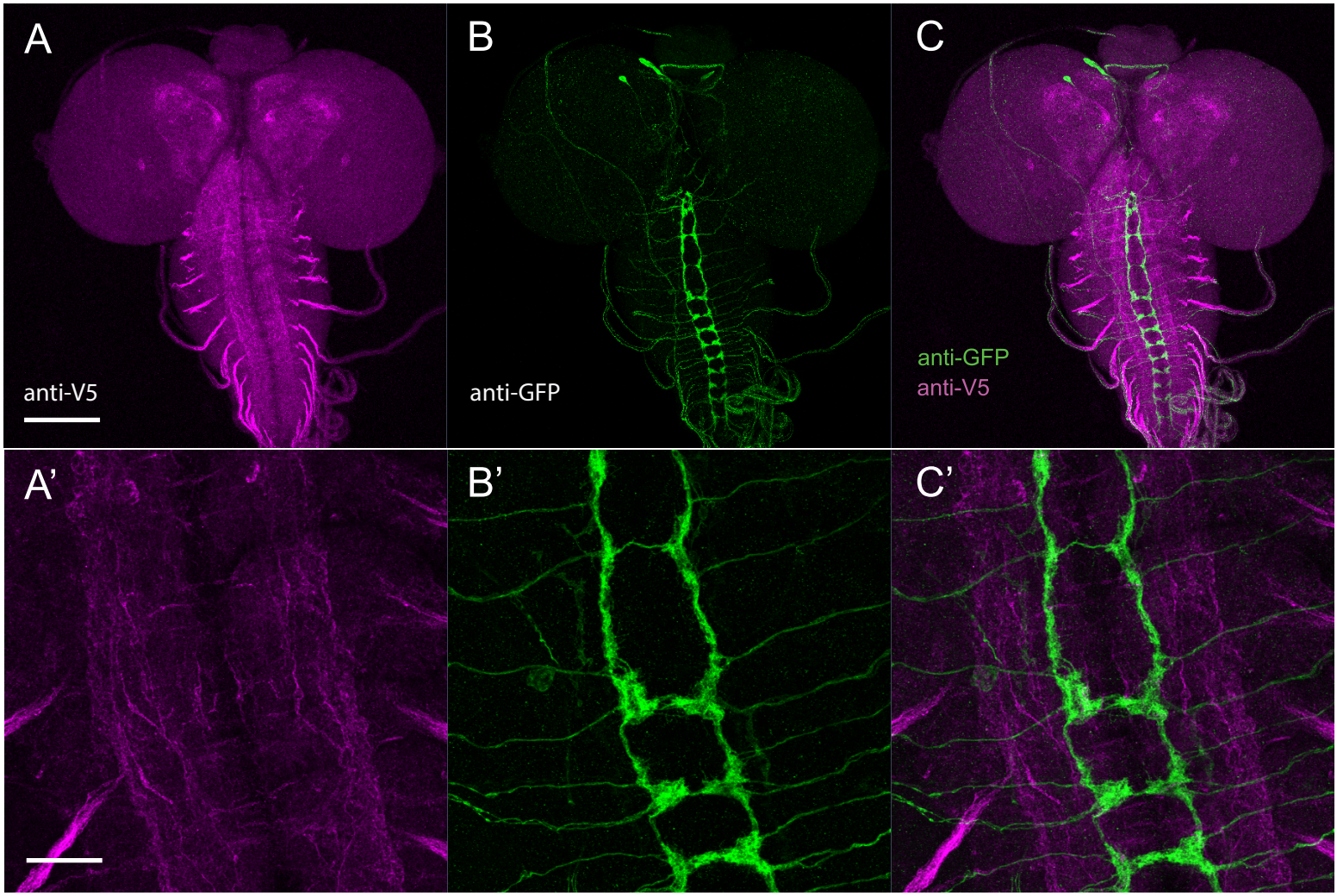

Figure S3. Immunostaining for SK::V5 proteins in larval brains. Related to Figure 4.
(A-C) Maximum intensity projection from z-stack images representative of larval brains. SK::V5 proteins do not localize to class IV axon terminals in the ventral nerve cord. SK::V5 protein expression (magenta in A,C) and Class IV projected terminals (green in B,C). Scale bars are 100μm. **(A'-C')** High magnification images of A, B, and C, respectively. Scale bars are 20μm.

Table S3. Oligonucleotide sequences. Related to STAR Methods

OLIGONUCLEOTIDE	SOURCE	ADDITIONAL INFORMATION
5'-GCAGTCGTGTATTTGCTGTCG-3'	IDT (This study)	Primer targeting *CanB* sequence flanking *SK* deletion (primer pair 1, Figure S1)
5'-TACTATTCCTTTCACTCGCACTTATTG-3'	IDT (This study)	Primer targeting residual *P{XP}* transposable element sequence flanking *SK* deletion (primer pair 1, Figure S1)
5'-ATGTCAATTCAGAAGCTTAACGACAC-3'	IDT (This study)	Primer targeting *SK* locus (primer pair 2, Figure S1)
5'-TGCAGTTGCTGCTGATGCAGAT-3'	IDT (This study)	Primer targeting *SK* locus (primer pair 2, Figure S1)
5'-TTATTCATGATAGATAACTGCGCTGACG-3'	IDT (This study)	Primer targeting *SK* locus (primer pair 3, Figure S1)
5'-CACCATGCCGCAGGTGAGGGTGATA-3'	IDT (This study)	Primer targeting *SK* locus (primer pair 3, Figure S1)
5'-CCTCGATATACAGACCGATAAAAC-3'	IDT (This study)	Primer targeting residual *pBac{WH}* transposable element sequence flanking *SK* deletion (primer pair 4, Figure S1)
5'-ATGCTGGTGCCCTACGATCTATGT-3'	IDT (This study)	Primer targeting remaining *SK* sequence flanking *SK* deletion (primer pair 4, Figure S1)
5'-CAACCGGATGTGAAGTGCG-3'	IDT (This study)	Primer targeting *Caα1D* sequence (control primer pair, Figure S1)
5'-CTTGGCACTTCGCCTGAAGG-3'	IDT (This study)	Primer targeting *Caα1D* sequence (control primer pair, Figure S1)
5'-ATGTCAATTCAGAAGCTTAACGAC-3'	IDT (This study)	Primer targeting *SK-M* mRNA isoform sequence for cDNA cloning (open reading frame)
5'-TCAGCTAGAATGTGGAAACAGCAT-3'	IDT (This study)	Primer targeting *SK-M* mRNA isoform sequence for cDNA cloning (open reading frame)

OLIGONUCLEOTIDE	SOURCE	ADDITIONAL INFORMATION
5'- ATGTCGCCGGCCTTCTGC-3'	IDT (This study)	Primer targeting *SK-V* mRNA isoform sequence for cDNA cloning (open reading frame)
5'-TCAGCTAGAATGTGGAAACAGCAT-3'	IDT (This study)	Primer targeting *SK-V* mRNA isoform sequence for cDNA cloning (open reading frame)
5'-CACCATGTCAATTCAGAAGCTTAACGAC-3'	IDT (This study)	Primer targeting *SK-M* mRNA isoform sequence for *pENTR* subcloning
5'-TCAGCTAGAATGTGGAAACAGCATG-3'	IDT (This study)	Primer targeting *SK-M* mRNA isoform sequence for *pENTR* subcloning
5'-CACCATGTCGCCGGCCTTCT-3'	IDT (This study)	Primer targeting *SK-V* mRNA isoform sequence for *pENTR* subcloning
5'-TCAGCTAGAATGTGGAAACAGCATGGGC-3'	IDT (This study)	Primer targeting *SK-V* mRNA isoform sequence for *pENTR* subcloning
5'-CCATTCAAGCGCCAACGCCC-3'	IDT (This study)	gRNA cloned into *pU6-BbsI-chiRNA* vector for CRISPR gene editing (*SK::V5* allele generation)
5'-GAGCGGATCGAGCAGCGGCGGAACTTTTTACATCCTGACACAGCTGCAGTTGCCCCCATTGGTAAGCCTATCCCTAACCCTCTCCTCGGTCTAGATTCTACGCAAGCGCCAACGCCCCAATCGATGTTCAATGCAGCGCCCATGCTGTTTCCACATTCTAGG-3'	IDT (This study)	ssODN donor repair template for CRISPR gene editing (*SK::V5* allele generation)
5'-GAGCGTTTAACCAACCTAGAG-3'	IDT (This study)	Primer targeting *SK* locus for XbaI PCR-RFLP analysis (*SK::V5* allele)
5'-GCAGTTAGTGTTCGTCCAAAG-3'	IDT (This study)	Primer targeting *SK* locus for XbaI PCR-RFLP analysis (*SK::V5* allele)